Robust OFDM-Based Synchronization Against Very High Fractional CFO and Time-Varying Fading

Kapseok Chang and Sangho Lee, *Member, IEEE*

***Abstract*—This article investigates the advantages and disadvantages of cell search for LTE and NR. This investigation enables us to design a couple of synchronization signals specified in frequency domain for a whole of cell search. For time/frequency synchronization and partial cell identification, to achieve both low complexity and robustness against very high carrier frequency offset (CFO) and time-varying fading, we propose a primary synchronization signal generated by the centrally symmetric concatenation of a Zadoff–Chu sequence and its modified sequence. Also, for final cell identification, to minimize intercell interference, we propose a secondary synchronization signal constructed by element-wise exclusive-OR operation of two different cyclic-shifted m-sequences. By complexity, intercell interference analysis, and accuracy-optimized searching description, as well as cell-search evaluation, we elucidate that the proposed scheme provides many advantages, such as lower complexity, immunity toward CFO and mobility, and shorter mean cell search time directly related with latency and battery life.**

***Index Terms*—Carrier frequency offset, cell search, frequency synchronization, mobility, orthogonal frequency division multiplexing (OFDM) system, time synchronization.**

I. Introduction

SINCE it was first specified by the Digital Audio Broadcasting standard in 1980s, orthogonal frequency division multiplexing (OFDM), a multicarrier transmission technology, has been adopted by mobile communication standards that secure global markets such as 4G long-term evolution (LTE) [1]–[3] and 5G new radio (NR) [4]. The main reason for employing OFDMs is that they can cope with harsh frequency-selective fading environments due to multipaths with only single-tap equalization. Channel equalization can be this simple because OFDM uses a number of modulated narrowband subcarriers in frequency domain (FD) instead of one rapidly modulated broadband signal in time domain (TD). However, the main challenge for OFDM-based systems is to achieve reliable time and frequency synchronization (TFS). Inadequate synchronization can result in intersymbol interference (ISI) and intercarrier interference (ICI) that severely degrade system performance [5], [6].

Manuscript received May 27, 2019; revised November 3, 2019; accepted December 5, 2019. Date of publication January 27, 2020; date of current version September 2, 2020. This work was supported in part by the Institute of Information and communications Technology Planning and evaluation grant funded by the Korea government under Grant 2019-0-00002, and in part by the Development of On-Time·On-Rate Wireless Access and Optical Edge Cloud Networking Technologies for High-Precision Services. *(Corresponding author: Kapseok Chang.)*

The authors are with the Electronics and Telecommunications Research Institute (ETRI), Daejeon 34129, Korea (e-mail: kschang@etri.re.kr; shlee@etri.re.kr).

Digital Object Identifier 10.1109/JSYST.2020.2964816

Time synchronization addresses the detection and tracking of sample timing offsets (STOs) due to random propagation delays and/or sampling frequency inconsistencies between transmitter and receiver including highly time-varying fading (i.e., Doppler effect). Frequency synchronization also addresses the detection and correction of carrier frequency offset (CFO) between transmitter and receiver due to oscillator mismatch. A cyclic prefix (CP) is added to each OFDM symbol to give a margin that the time range from which ISI and ICI do not occur. Typically, the margin is within half of absolute CP duration, so that above ISI and ICI do not occur if the STO estimated is within the margin [5].

As with other wireless communication systems, all user equipments (UEs) seeking initial access to LTE and NR systems shall first perform the above-mentioned TFSs using specified primary synchronization signal (PSS). In addition to TFS, they shall perform serving physical cell identity (PCI) acquisition using specified secondary synchronization signal (SSS) with an aid of PSS. These two processes of synchronization in LTE and NR are specially called *cell search* due to additional PCI acquisition. Cell search in each of LTE and NR starts when UE synchronizes to the base station (BS) of serving cell. However, since UE is unable to know the carrier frequency of BS and able to move very fast, up to 500 km/h [4], its received signal can experience high CFO and time-variant distortion, respectively, which leads to causing unavoidable ICIs. Therefore, since initial time synchronization is performed prior to frequency synchronization with unknown mobility, it is pivotal to design synchronization signals and/or time synchronization algorithms that are robust against these unavoidable ICIs [6].

In the literature, various cell-search studies have been conducted [7]–[23] regarding TFS and PCI acquisition. Authors in [7]–[15] proposed substantive TFS schemes to acquire both time and frequency synchronization to comply with LTE and NR.[1] It was recommended that to improve timing accuracy, cross-correlation-based scheme[2] should be applied rather than autocorrelation-based scheme.[3] However, cross-correlation has two problems: First, for large CFO and high-speed mobility, the timing accuracy of cross correlation is significantly lower than that of autocorrelation, which is why we use autocorrelation for coarse time synchronization. Second, even for negligible CFO and nomadic mobility, the computational complexity to perform cross correlation is significantly higher than that of autocorrelation, while the timing accuracy of cross correlation is far superior to that of auto correlation. Accordingly, developing a scheme

[1]Descriptions regarding these studies will be discussed in Section II.

[2]It uses the correlation of a received signal with a synchronization signal.

[3]It uses the correlation of a received signal with a form of itself that is behind in time.

reducing the complexity involved in cross correlation at receiver is important, but it is pivotal to design a synchronization signal harmonizing with existing cross-correlation schemes [7]–[15] at receiver to achieve high timing accuracy and low correlation complexity at the same time. Authors in [16]–[18] carried out studies designing synchronization signals themselves for cross correlation. However, the synchronization signals designed are not necessary to realize the simultaneous achievement.

On the other hand, authors in [19]–[23] proposed substantive schemes to acquire PCI using SSS with the help of PSS to comply with LTE and NR. An LTE synchronization signal (SS) block of adjacent SSS and PSS every half frame is transmitted so that LTE specified swapping method [19] in SSS for frame synchronization (FS) to determine whether the first half or the second half is the frame. However, this swapping method causes double collision problem, which results in huge intercell interference. To lower collision probability, both PSS- and SSS-specific scrambling are additionally employed in SSS [1], [6], but still there exists collision probability. Also, the normalized cross correlation of two different SSS signals is as high as 0.5, which leads to a high probability of wrong PCI acquisition in low signal-to-noise ratio (SNR) [22]. To improve PCI acquisition accuracy at receiver in LTE, authors [20], [21] proposed maximum likelihood (ML) schemes based on correcting channel distortions in SSS using the channel state information estimated from adjacent PSS. Moreover, regarding NR, even though it is revolved and not backward compatible with LTE, similar synchronization functionality except for no such FS owing to supporting beam sweeping [22], [23] is adopted. By this reason, one SS block for certain beam direction may be transmitted every 20 ms in worst case, so that decent one-shot PCI acquisition performance is guaranteed using SSS in NR. For intercell interference mitigation, NR is designed with no collision probability between any pairs of two SSS signals. Authors in [22] demonstrated the superiority of NR SSS over LTE SSS, but a fair comparison in terms of resource usage for each 10-ms frame is further required.

Contribution to previous work: To realize low-complexity and accuracy cell search, with accuracy-optimized searching description, we concentrate on proposing robust PSS and SSS signals which can be even so harmonized with the aforementioned detection schemes [7]–[15], [20], [21]. In the sequel for the convenience of explanation, the system employing the proposed SS block is called alternative radio (AR) to distinguish it from LTE and NR. We sum up our contributions as follows.

1) We propose a new FD signal of PSS, the centrally symmetric concatenation (CSC) of a Zadoff–Chu (ZC) sequence and its modified sequence, for TFS and partial PCI acquisition (as in LTE and NR) named *Step-1 cell search*. The purpose of this PSS is to be robust against CFO and mobility in parallel with lowering computational complexity on *Step-1* searcher. To achieve this purpose, we will prove that the TD signal corresponding to the PSS FD signal of AR is real, so that it lowers computational complexity. Also, a selection metric based on 2 stages will be proposed to effectively pick three best PSS sequence indexes to show robustness against high fractional CFO.
2) A new FD signal of SSS, an element-wise exclusive-OR operation of two different cyclic-shifted m-sequences carrying PCI without requiring any scrambling sequence is proposed for final PCI acquisition (as in NR) named *Step-2 cell search*. The purpose of this SSS is to not only resolve the collision problem mentioned in [19] and [24] but also minimize intercell interference in parallel with reduction in hardware complexity on Step-2 searcher. To achieve this purpose, we will analyze collision probability, hardware complexity, and analytic simplified cross-correlation property.
3) This article will make a fair comparison of the cell-search performance of AR with those of LTE and NR in terms of resource use per frame (i.e., the same number of resource elements used for each 10-ms frame) in the presence of up-to high CFO and mobility.

The remainder of this article is organized as follows. Section II describes previous studies related with TFS. We describe system for this article in Section III. We model the SS blocks of LTE, NR, FD-version [18], and AR, analyzing a selection metric of AR PSS sequence index and comparative analyses regarding PSS and SSS specifications in Section IV. Section V describes Step-1 and Step-2 searchers with analyzing searcher complexity and depicting average cell-search time. In Section VI, through evaluation, we compare AR with LTE, NR, and the FD-version in terms of detection error rate (DER) and average search time, followed by conclusions drawn in Section VII.[4]

II. Related TFS Synchronization Studies

Literature in [7]–[15] proposed substantive TFS schemes to acquire both time and frequency synchronization to comply with LTE and NR (i.e., there was no modification to the PSS signals themselves in LTE and NR): Mansour [7] proposed a hardware-efficient scheme to compute ZC sequence elements in both of time domain and frequency domain using simple duality relationship for time synchronization in LTE; Xu and Manolakis [8] proposed an effective TFS algorithm using PSS in LTE, where autocorrelation using CP was first performed, and cross correlation using PSS was carried out; Zhang *et al.* [9] proposed a useful time-synchronization scheme that utilizes the central-symmetric property of the TD ZC signal to minimize cross-correlation complexity on the PSS signal in LTE; Yuan and Torlak [10] proposed an ML scheme for joint CFO and sampling frequency offset estimation exploiting the fact that a single source such as crystal oscillator belonging to a BS is typically used to provide a reference frequency for both sampling clock and radio frequency synthesizers; Morelli and Moretti [11] proposed a novel TFS algorithm relying on ML estimation criterion and exploiting a reduced-rank representation of the channel frequency response; Lin *et al.* [12] proposed a TFS algorithm to exploit multi-sector diversity in LTE, taking into account inter-cell interference, ICI, and multipath; Hu and Zhang [13] reduced the number of multiplication operations on performing TFS using not modification but feature for the time-domain PSS specification of NR; Abdzadeh-Ziabari *et al.* [14] proposed joint ML estimation of timing and CFO exploiting basis expansion modelling capturing the time variations of the channel, where this estimation has an advantage in high-speed mobile situations; Zeng *et al.* [15] regarding frequency synchronization proposed separate estimates of CFO and Doppler shift based on orthogonal angle-domain subspace projection at very high mobility (e.g., up to 500 km/h in NR). On the other hand, rather than TFS studies at receiver, literature in [16]–[18] carried out

[4]We list the abbreviations and notations used throughout this article as shown in Table I.

TABLE I
LIST OF ALPHABETICAL-ORDER ABBREVIATIONS INCLUDING NOTATIONS

Acronym/Notation	Explanation
AR	Alternative Radio
AST	Average Search Time
BPSK	Binary Phase Shift Keying
BS	Base-Station
CFO	Carrier Frequency Offset
CGI	Cell Group Identity
CP	Cyclic Prefix
CSC	Centrally Symmetric Concatenation
DC	Direct Current
DER	Detection Error Rate
EAC	Effective Accumulated Cross-correlation
EMA	Effective Margin Accumulation
FD	Frequency Domain
FFT	Fast Fourier Transform
ICI	Inter-Carrier Interference
IFFT	Inverse Fast Fourier Transform
ISI	Inter-Symbol Interference
LTE	Long-Term Evolution
ML	Maximum Likelihood
MOPS	Millions of Operations Per Second
NR	New Radio
OFDM	Orthogonal Frequency Division Multiplexing
PCI	Physical Cell Identity
PID	Physical Identity
PN	Pseudo-Noise
PSS	Primary Synchronization Signal
SNR	Signal-to-Noise Ratio
SS	Synchronization Signal
SSS	Secondary Synchronization Signal
SSTP	Starting Sample Time of PSS TD signal
STO	Sample Time Offset
TD	Time Domain
TFS	Time/Frequency Synchronization
UE	User Equipment
ZC	Zadoff-Chu
$\mathbf{v}^T$	The transpose of a vector $\mathbf{v}$
$\mathbf{V}^H$	The complex conjugate transpose of a matrix $\mathbf{V}$
$(\mathbf{v})_m$	The m-th component of a vector $\mathbf{v}$
$(\mathbf{M})_{m,n}$	The (m,n)-th element of matrix $\mathbf{M}$
$E\{x\}$	The expectation of random variable x
$\mathbf{0}_n$	The $1\times n$ zero vector
$\delta(\cdot)$	Kronecker delta function
$[y]_m$	The modulo-m of y, where $[y]_m = [m+y]_m$ for negative integer y
$\lfloor y \rfloor$	The largest integer less than or equals real number y

studies designing synchronization signals themselves for cross correlation: Chang and Han[16] modified FD-based PSS in LTE and performed a replica correlation to acquire TFS and partial PCI, where they succeeded in improving timing accuracy even at high CFO without minimizing computational complexity; Chang *et al.* [17] has designed an accurate and low-complexity FD PSS signal, where it is not true that this low complexity is guaranteed regardless of inverse fast Fourier transform (IFFT) size; Gul *et al.* [18] proposed a TD structure of two consecutive ZC-based synchronization signals for time and frequency synchronization.

Once again, developing further optimal TFS scheme reducing the complexity of cross correlation at receiver is an option, but it may be mandatory to design a synchronization signal harmonizing with existing TFS schemes highly optimized as in [7]–[15] to achieve high timing accuracy and low correlation complexity at the same time. However, the synchronization signals designed in [16]–[18] are insufficient to satisfy both high accuracy and low complexity. In addition, the PSS signals specified in all of [16] and [17], LTE, and NR are occupying not a whole of feasible subcarriers, but partial subcarriers in frequency domain, and the rest of subcarriers are allocated to data/control channels as shown in Fig. 1 to enhance resource efficiency. Unlike in [16] and [17], since the synchronization signals in [18] are allocated to time domain, they are occupying a whole of subcarriers. Accordingly, there is an issue of not being able to use resources efficiently in [18].

III. SYSTEM DESCRIPTION

As shown in Fig. 1, for a fair comparison with LTE [1] and NR [4] in terms of resource use per frame and multiple-carrier transmission method, the AR system considered in this article employs OFDM. Besides, every 10 ms constitutes a frame structure in which a pair of PSS and SSS adjacent to each other in time domain is allocated at the center of system bandwidth as in LTE. A frame is composed of ten subframes. Each of subframe consists of two time slots, each of which comprises 7 OFDM symbols, so that the number of symbols corresponding to one subframe is 14 (i.e., $l = 0, 1, 2, \ldots, 13$). In time domain, SSS and PSS are located in the second last and last symbols (i.e., $l = 5$ and 6), respectively, in only Slot 0.[5] On the other hand in frequency domain, these signals occupy $2N_p + 1$ subcarriers (i.e., $k = 0, 1, 2, \ldots, 2N_p$, where $N_p = 63$) including direct current (dc) subcarrier. Also, when subcarrier spacing is assumed to be 15 kHz, the minimum downlink sampling rate at transmitter for PSS and SSS in Fig. 1 is 3.84 MHz which sets the IFFT size[6] N to be 256, and the CP duration N_{cp}^l to be 20 for symbols $l = 0, 7$ and 18 for symbols $l = 1, 2, \ldots, 6, 8, 9, \ldots, 13$.

Let $X_{f',f}^{c,l}[k]$ be the baseband transmit (Tx) AR frequency-domain signal related with synchronization signals, where f, $f'(= 0, 1, \ldots, 9)$, and $c(= 0, 1, \ldots, Q \times G - 1)$ stand for frame, subframe, and PCI indexes, respectively. In PCI c, the number of physical identities (PIDs) Q and that of cell group identities (CGIs) G each are 3 and 336 as in NR. The corresponding baseband Tx time-domain signal $\tilde{x}_{f',f}^{c,l}[n]$ for $0 \le n < (N_{cp}^l + N)$ is expressed as, in accordance with allocation at the center of system bandwidth like the standard of LTE

$$\tilde{x}_{f',f}^{c,l}[n] = \sum_{k'=-N_p}^{N_p} X_{f',f}^{c,l}[k] e^{j\frac{2\pi k(n-N_{cp}^l)}{N}} \tag{1}$$

where $X_{f',f}^{c,l}[k]$ can be either $S_{0,c}[k]$ or $P_{0,u}[k]$ with $k = k' + N_p$ in range of 0 to $2N_p$ as shown in Fig. 1, $X_{f',f}^{c,l}[N_p] = 0$, and $E\{|\tilde{x}_{f',f}^{c,l}[n]|^2\} = E_s$, E_s being the average Tx power. The $(N + N_{cp}^l) \times 1$ vector form of (1) is expressed again as

$$\tilde{\mathbf{x}}_{f',f}^{c,l} = \mathbf{F}_- \underbrace{\left[\mathbf{X}_{f',f,+}^{c,l} \mathbf{0}_{\frac{N}{2}+1} \mathbf{X}_{f',f,-}^{c,l}\right]^T}_{\mathbf{X}_{f',f}^{c,l}\text{: IFFT input}} = \left[\mathbf{x}_{cp,f',f}^{c,l} \mathbf{x}_{f',f}^{c,l}\right]^T$$

$$\mathbf{X}_{f',f,+}^{c,l} = \left[X_{f',f}^{c,l}[N_p] X_{f',f}^{c,l}[N_p+1] \cdots X_{f',f}^{c,l}[2N_p]\right]$$

$$\mathbf{X}_{f',f,-}^{c,l} = \left[X_{f',f}^{c,l}[0] X_{f',f}^{c,l}[1] \cdots X_{f',f}^{c,l}[N_p-1]\right] \tag{2}$$

[5]For fair comparison of resource usage per frame, it is assumed in this article that while LTE transmits a pair of SSS and PSS every 5 ms as it is, AR transmits a pair of SSS and PSS every 10 ms.

[6]While $N = 256$ in NR as AR, $N = 128$ in LTE at 1.92 MHz sampling rate.

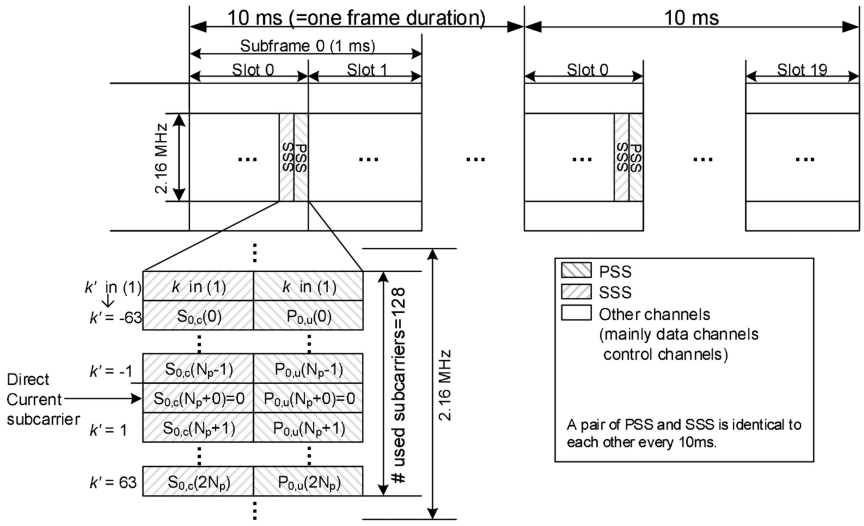

Fig. 1. Frame structure considered in this article.

where $\mathbf{0}_{N/2+1}$ is the $(1 \times (N/2+1))$ zero vector, and $\mathbf{F}_-$ is an $(N + N_{cp}^l) \times N$ IFFT matrix given as the (m,n)th element of $\mathbf{F}_-$, i.e., $(\mathbf{F}_-)_{n,m} = \exp\{j2\pi(n - N_{cp}^l)m/N\}$ for $0 \le n < (N + N_{cp}^l)$ and $0 \le m < N$. In (2), $\mathbf{x}_{cp,f',f}^{c,l}$ and $\mathbf{x}_{f',f}^{c,l}$ each are the $(1 \times N_{cp}^l)$ and $(1 \times N)$ baseband Tx time-domain signal vectors corresponding to CP and effective OFDM symbol.

Letting us assume a frequency-selective fading channel with time variance, the $(N + N_{cp}^l) \times 1$ baseband receive (Rx) signal vector $\tilde{\mathbf{r}}_{l,f',f}^a$ coping with $\tilde{\mathbf{x}}_{f',f}^{c,l}$ in (2) is

$$\tilde{\mathbf{r}}_{l,f',f}^a = \mathbf{E}_{l,f',f}^{c,a}\mathbf{H}_{l,f',f}^{c,a}\tilde{\mathbf{x}}_{f',f}^{c,l} + \sum_{c' \ne c}\left\{\mathbf{E}_{l,f',f}^{c,'a}\mathbf{H}_{l,f',f}^{c,'a}\tilde{\mathbf{x}}_{f',f}^{c,'l}\right\} + \left[\mathbf{z}_{l,f',f}^{cp,a}\mathbf{z}_{l,f',f}^{a}\right]^T = \left[\mathbf{r}_{l,f',f}^{cp,a}\mathbf{r}_{l,f',f}^{a}\right]^T \quad (3)$$

where a stands for Rx antenna index with $a = 0, 1, \ldots, A-1$, $\mathbf{r}_{l,f',f}^{cp,a}$ and $\mathbf{r}_{l,f',f}^{a}$ are the $(1 \times N_{cp}^l)$ and $(1 \times N)$ baseband Rx time-domain signal vectors corresponding to CP and effective OFDM symbol, respectively, and $\mathbf{z}_{l,f',f}^{cp,a}$ and $\mathbf{z}_{l,f',f}^{a}$ are the $(1 \times N_{cp}^l)$ and $(1 \times N)$ complex Gaussian random variable vectors corresponding to CP and effective OFDM symbol, respectively, with zero mean and variance N_0. In (3), $\mathbf{E}_{l,f',f}^{c,a}$ is the $(N + N_{cp}^l) \times (N + N_{cp}^l)$ diagonal matrix related with CFO given by $\mathbf{E}_{l,f',f}^{c,a} = \text{diag}\{E_{l,f',f}^{c,a}(0) \ldots E_{l,f',f}^{c,a}(N + N_{cp}^l - 1)\}$, where $E_{l,f',f}^{c,a}(n) = \exp\{j2\pi\varepsilon_c n/N\}$ with the CFO ε_c between transmitter and receiver normalized to a subcarrier spacing in c. Also, $\mathbf{H}_{l,f',f}^{c,a}$ is the $(N + N_{cp}^l) \times (N + N_{cp}^l)$ time-impulse-response matrix of time-variant channel given by $(\mathbf{H}_{l,f',f}^{c,a})_{n,k} = h(n, [n-k]_{N+N_{cp}^l})$ for $0 \le n, k < N + N_{cp}^l$, from [25], with the time-variant path gain $h(n, \xi)$ of the ξth multipath component normalized by sample time n. Moreover, the second term of the first line in (3) is introduced to represent interferences coming from neighbor cells.

IV. Signal Description and Analysis

This section, first with an aid of (1) and Fig. 1, describes the SS blocks of LTE, NR, [18],[7] and AR allocated to frequency domain, where NR, [18], and AR set $N_p = 63$ and $G = 336$ while LTE sets $N_p = 31$ and $G = 168$, and all of LTE, NR, and AR share $Q = 3$ commonly. Specifically, CGI $g = \lfloor c/Q \rfloor$ in PCI c, and PID $u = [c]_Q$ identifying one of Q cells within each CGI g, so that PCI c can be regenerated as $c = 3g + u$. Second, we present 2-Stage metric to select three root indexes of AR PSS sequence suitable for PIDs. Third, to prove the excellence of the AR SS block proposed in this article, we make comparative PSS analyses such as complexity and robustness against CFO and mobility, as well as comparative SSS analyses such as collision probability and analytic simplified cross correlation.

A. LTE Synchronization Signal Description

Specifically, the PSS FD signal $P_{f',u}[k]$ for $f' = 0, 5$ and $l = 6$ [1] is given by

$$P_{f',u}[k] = X_{f',f}^{c,6}[k] = \exp\left\{-j\frac{\pi\mu_u k(k+1)}{2N_p+1}\right\} \; 0 \le k < 2N_p+1 \quad (4)$$

where $P_{0,u}[k] = P_{5,u}[k]$, $P_{0,u}[N_p] = 0$, and μ_u is the root index of length-$(2N_p + 1)$ ZC sequence corresponding to PID u with $\mu_0 = 25$, $\mu_1 = 29$, and $\mu_2 = 34$.

Specifically, the SSS FD signal is given by $S_{f',c}[k] = X_{f',f}^{c,5}[k]$ for $f' = 0, 5$ and $l = 5$. $S_{f',c}$ is constructed from the first length-N_p scrambling pseudonoise (PN) sequences e_0 and e_1 determined by PID u, the interleaved length-N_p short PN sequences b_{i_0} and b_{i_1} determined by CGI g, and the secondary length-N_p scrambling PN sequences w_{i_0} and w_{i_1} determined by b_{i_0} and

[7] In this article, to address the issue at the end of Section II the TD training signal proposed in [18] is allocated to partial subcarriers as in Fig. 1 for the sake of fair comparison in terms of resource use. In addition, it is noted only the first training signal as in (8) is employed because only fractional CFOs are considered.

b_{i_1}, as follows:[8]

$$S_{f',c}[k] = \begin{cases} b_{i_{\lfloor f'/5 \rfloor}}[\tilde{k}]e_0[\tilde{k}], & 0 \le \text{even } k < N_p \\ b_{i_{[\lfloor (f',x+5)/2 \rfloor]_2}}[\tilde{k}]e_1[\tilde{k}]w_{i_{\lfloor f'/5 \rfloor}}[\tilde{k}] & 0 \le \text{ odd } k < N_p \\ b_{i_{[\lfloor (f'+5)/2 \rfloor]_2}}[\tilde{k}]e_1[\tilde{k}]w_{i_{\lfloor f'/5 \rfloor}}[\tilde{k}], & N_p+1 \le \text{even } k \le 2N_p \\ b_{i_{\lfloor f'/5 \rfloor}}[\tilde{k}]e_0[\tilde{k}] & N_p+1 \le \text{ odd } k \le 2N_p \end{cases} \quad (5)$$

where $\tilde{k} = \lfloor k/2 \rfloor$. As (5) suggests, b_{i_0} and b_{i_1} in subframe $f' = 0$ are swapped in subframe $f' = 5$.

B. NR Synchronization Signal Description

Specifically, the PSS FD signal $P_{0,u}[k]$ in $l = 6$ for $0 \le k < 2N_p + 1$ [4] as shown in Fig. 1 is given by, based on binary phase shift key (BPSK)-modulated length-$(2N_p + 1)$ PN sequence that is reused in SSS for reducing hardware complexity

$$\begin{aligned} P_{0,u}[k] = X_{0,f}^{c,6}[k] &= \left[1 - 2x_0\left([k+\mu_u]_{2N_p+1}\right)\right] \\ x_0(i+7) &= [x_0(i+4) + x_0(i)]_2 \\ [1110110] &= [x_0(6)x_0(5)x_0(4)x_0(3)x_0(2)x_0(1)x_0(0)]. \end{aligned} \quad (6)$$

Here it is necessary to note that according to the specification of NR [4], a pair of PSS and SSS for a particular direction is transmitted every 20 ms. However, for a fair cell-search performance comparison with LTE in terms of resource use per frame and resource allocation position, the pair is assumed to be transmitted every frame, and the FD resource for PSS is centrally allocated, so that $P_{0,u}[N_p] = 0$ in (6) due to dc. Also, μ_u in (6) is the cyclic shift index of the PN sequence x_0 corresponding to PID u with $\mu_0 = 0$, $\mu_1 = 43$, and $\mu_2 = 86$.

Specifically, the SSS FD signal $S_{0,c}[k] = X_{0,f}^{c,5}[k]$ in $l = 5$ for $0 \le k < 2N_p + 1$ is constructed from an element-wise multiplication of two different BPSK-modulated length-$(2N_p + 1)$ cyclic-shifted PN sequences x_0 and x_1 as follows:

$$\begin{aligned} S_{0,c}[k] &= [1 - 2x_0([k+m_0]_{127})][1 - 2x_1([k+m_1]_{127})] \\ g_0 &= \lfloor g/112 \rfloor (= 0,1,2), g_1 = [g]_{112} (= 0,1,\ldots,111) \\ m_0 &= 15g_0 + 5u, m_1 = g_1 \\ x_0(i+7) &= [x_0(i+4) + x_0(i)]_2 \\ x_1(i+7) &= [x_7(i+1) + x_1(i)]_2 \\ [0000001] &= [x_0(6)x_0(5)x_0(4)x_0(3)x_0(2)x_0(1)x_0(0)] \\ [0000001] &= [x_1(6)x_1(5)x_1(4)x_1(3)x_1(2)x_1(1)x_1(0)] \end{aligned} \quad (7)$$

where PCI c is obtained by a regeneration of two different cyclic-shift indexes m_0 and m_1. In other words, CGI g is mapped out g_0 in m_0 and g_1 in m_1 in a distributed manner, and PID u is mapped into m_0, so that PCI c is got as $3g + u$.

[8]It is noted that the mathematical expression of SSS signal in (5) looks different from that in LTE, but is exactly identical to each other since it comes from simply including dc subcarrier when indexing.

C. FD-Version Synchronization Signal Description [18]

Specifically, the PSS FD signal $P_{0,u}[k]$ in $l = 6$ for $0 \le k < 2N_p + 1$ [18] as shown in Fig. 1 is given by, based on length-$(2N_p + 2)$ ZC sequence

$$P_{0,u}[k] = X_{0,f}^{c,6}[k] = \exp\left\{ j\frac{\pi\mu_u k^2}{2N_p+2} \right\} \quad (8)$$

where $P_{0,u}[N_p] = 0$ due to dc. According to preliminary evaluation, μ_u in (8) is set to $\mu_0 = 1$, $\mu_1 = 25$, and $\mu_2 = 43$ corresponding to PID u.[9]

D. AR Synchronization Signal Description

Let us propose not only a PSS FD signal based on centrally symmetric concatenation of base sequence and its modified sequence but also an SSS FD signal based on element-wise exclusive-OR operation of two different PN sequences.[10]

First, the PSS FD signal $P_{0,u}[k]$ for $l = 6$ and $0 \le k < 2N_p + 1$ is constructed from a CSC of length-N_p complex ZC sequence b_u and its conjugated sequence $\tilde{b}_u$ as

$$\begin{aligned} P_{0,u}[k] &= \begin{cases} \tilde{b}_u[N_p - 1 - k], & 0 \le k < N_p \\ b_u[k - N_p - 1], & N_p + 1 \le k \le 2N_p \end{cases} \\ \text{with } b_u[k] &= \exp\left\{ -j\frac{\pi\mu_u k(k+1)}{N_p} \right\}, 0 \le k < N_p \\ \tilde{b}_u[k] &= b_u^*[k], 0 \le k < N_p \end{aligned} \quad (9)$$

where $P_{0,u}[N_p] = 0$, and μ_u is the root index of the length-N_p ZC base sequence (to be determined in Subsection IV-E).

Second, the SSS FD signal $S_{0,c}[k] = X_{0,f}^{c,5}[k]$ in (1) for $l = 5$ and $0 \le k < 2N_p + 1$ is constructed from an element-wise exclusive-OR operation of two different cyclic-shifted length-$2N_p + 1$ PN sequences x_0 and x_1 as follows:

$$\begin{aligned} S_{0,c}[k] &= 1 - 2\left[x_0\left([k+m_0]_{127}\right) \oplus x_1\left([k+m_1]_{127}\right)\right] \\ g &= \lfloor c/3 \rfloor, u = [c]_3 \\ g_0 &= \lfloor g/28 \rfloor (= 0,1,\ldots,11), g_1 = [g]_{28} (= 0,1,\ldots,27) \\ m_0 &= 3\left(g_0 + 12u\right), \quad m_1 = 2g_1 \\ x_0(i+7) &= [x_0(i+4) + x_0(i)]_2 \\ x_1(i+7) &= [x_7(i+1) + x_1(i)]_2 \\ [0000001] &= [x_0(6)x_0(5)x_0(4)x_0(3)x_0(2)x_0(1)x_0(0)] \\ [0000001] &= [x_1(6)x_1(5)x_1(4)x_1(3)x_1(2)x_1(1)x_1(0)] \end{aligned} \quad (10)$$

where PCI c is obtained in the same way as (7). In (10), the scaling factors 3 and 2 in m_0 and m_1 are introduced to ensure the robustness of the SSS signal itself (refer to [22]) against carrier frequency offset.

[9]In this article, since maximum allowable CFO is not assumed to be beyond subcarrier spacing according to [22] and the focus is on optimizing cross correlation as mentioned in Sections I and II, the second training symbol of [18] is not taken into account.

[10]As complex and binary sequences, well-known complex ZC and binary PN sequences [1], [26], are employed as examples in this article for the proposed synchronization signal design. On that account, any complex and binary sequences are capable of being applied if those demonstrate sufficient correlation properties.

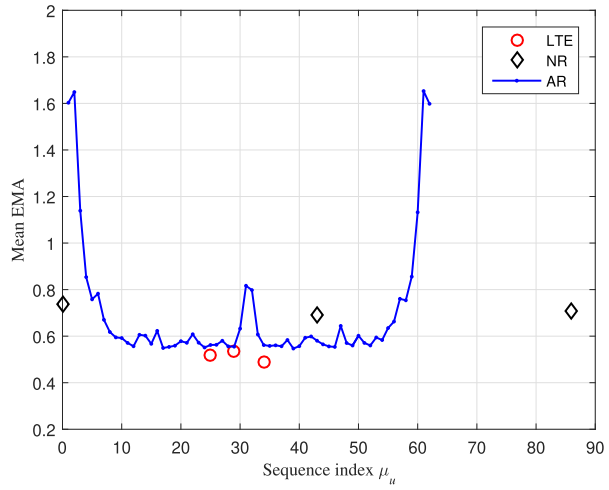

Fig. 2. Mean EMA vs. sequence index at Stage 1 with a maximum tolerable CFO = 5.05 ppm [22] for a carrier frequency of 2 GHz.

E. 2-Stage Selection Metric of AR PSS Sequence Index

Let us answer the question "How should we select the best three root indexes from the proposed AR PSS sequence?". If there exists a CFO between transmitter and receiver, this CFO will cause a timing error. However, it is fortunate that any intersymbol interference does not occur at all, as long as the timing error is within $\pm\lfloor N_{cp}^6/2\rfloor$ [27]. This fortune enables us to present the following metric based on 2 stages in the presence of high CFO.

Stage 1: To analyze robustness against CFO, we define one effective margin accumulation (EMA) as the summated absolute cross-correlation output within half CP duration

$$\mathrm{EMA}(\mu_u) = \frac{1}{N}\sum_{\varphi'=-\lfloor N_{cp}^6/2\rfloor}^{-1} \times \left|(\breve{\mathbf{r}}_{6,0,f}^{0,\mu_u})^T\left(\varphi'+N_{cp}^6\right)\cdot(\breve{\mathbf{r}}_{6,0,f}^{0,\mu_u})^*\left(N_{cp}^6\right)\right| \tag{11}$$

where one Rx antenna is assumed [i.e., $A=1$ in (3)], $\breve{\mathbf{r}}_{6,0,f}^{0,\mu_u}(\varphi)$ with $u=[c]_Q$ is the component vector of $\tilde{\mathbf{r}}_{l,f',f}^0$ excluding interference(2nd term) and noise(3 rd term) from (3), and the PSS FD signal applied to $\tilde{\mathbf{x}}_{f',f}^{c,l}$ of (3) is that in AR as shown in (9). Also, in (11), the meaning of $\cdot(\varphi)$ is that vector $\breve{\mathbf{r}}_{6,0,f}^{0,\mu_u}(\varphi)$ is the $(1\times N)$ vector extracted from starting element φ of $\breve{\mathbf{r}}_{6,0,f}^{0,\mu_u}$. For illustration purpose, we consider no interfering cell without noise. However, for the consistency of analysis in the same line with evaluation in Section VI, this article applies 6-tap Typical Urban (TU-6) fading channel [29] to $h(n,\xi)$ in (3) with 3 km/h mobility, and a maximum tolerable CFO of 10.1 kHz (i.e., $\varepsilon_c=0.6733$ coping with 5.05 ppm at carrier frequency of 2 GHz) to $\mathbf{E}_{l,f',f}^{c,a}$ in (3). The mean EMA performance is shown in Fig. 2, as a function of the sequence index with which μ_u is replaced in (9). From the results of this figure, we select sequence indexes 1, 2, 3, 60, 61, 62 such that the mean EMA of the proposed signal is very higher than those of LTE and NR. Fundamentally, there are 120 candidate sets each of which comprises 3 indexes, i.e., μ_0, μ_1, and μ_2, but since indexes 2 and 61 have very dominant EMAs, these are selected by default in this article. According to this, we retain only four candidate sets: {1, 2, 61}, {2, 3, 61}, {2, 60, 61}, and {2, 61, 62}.

TABLE II
MEAN EAC RESULTS

$(\mu(u,\mu_u'))$	$E\{\Lambda\}$	$(\mu(u,\mu_u'))$	$E\{\Lambda\}$	$(\mu(u,\mu_u'))$	$E\{\Lambda\}$
(2,61)°	0.0364	(2, 3)	0.0382	(61,62)	0.0371
(2, 1)°	0.0358	(2,60)	0.0342	(61, 3)	0.0333
(2,62)	0.0484	(61,1)°	0.0372	(61,60)	0.0333

TABLE III
SIGNAL TYPE OF PSS TD SIGNAL

	$N=64$	$N\geq 128$
LTE	complex	complex
NR	(complex)*	complex
FD-version [18]	(complex)*	complex
AR	(real)*	real

* (y) means it is not specified, but fundamentally classified as string "y".

Stage 2: Under the same condition as Stage 1, we define another effective accumulated cross correlation (EAC) as

$$\Lambda(\mu_u,\mu_u') = \frac{1}{N}\sum_{\varphi'=-\lfloor N_{cp}^6/2\rfloor}^{-1}\left|(\breve{\mathbf{r}}_{6,0,f}^{0,\mu_u})^T\left(\varphi'+N_{cp}^6\right)\cdot(\breve{\mathbf{r}}_{6,0,f}^{0,\mu_u'})^*\left(N_{cp}^6\right)\right| \tag{12}$$

where μ_u is different from μ_u'. From the mean EAC performance shown in Table II, subsequently, we found the best index set {1, 2, 61}. The criterion to select this set in this table is that the lower the mean EAC value, the better the cross correlation, and as the gap among mean EAC values selected is close to zero, remaining intercell interference becomes fair.

F. Comparative Analysis Regarding PSS Specification

First, let us compare the AR PSS time-domain signal with existing PSS time-domain ones in terms of signal type that are summarized in Table III according to IFFT size N, which will be revisited when we say searcher's complexity. Regarding the proposed PSS TD signal, it is fundamentally real regardless of IFFT size N. We have the following proposition:

Regarding LTE, NR, and [18], their PSS TD signals are complex regardless of IFFT size, which is coming from the IFFT property [26] that the TD signal of the FD signal consisting either one base ZC complex signal or one base binary m-sequence is complex. In contrast, the proposed PSS TD signal is real regardless of IFFT size N. We have the following proposition.

Proposition 1: The TD signal corresponding to $P_{0,u}[k]$ in (9) is real.

Proof: See Appendix A. ■

Second, under the same condition as Section IV-E, the robustness of CFO is analyzed based on a couple of average EMA and average EAC for each of LTE, NR, [18], and AR, where AR PSS sequence index μ_u is selected to be 1, 2, and 61. The meaning of average EMA and average EAC in Table IV is the averages of three mean EMAs and EACs corresponding to μ_u mentioned in Stages 1 and 2, respectively. From this table, it is observed that AR outperforms, followed by NR, because the bigger the average EMA and the smaller the average EAC, the higher the robustness

TABLE IV
SUMMARY ON ROBUSTNESS AGAINST CFO

	Average EMA	Average EAC
LTE	0.5144	0.0883
NR	0.7125	0.0376
FD-version [18]	0.6121	0.0532
AR	1.6349	0.0368

TABLE V
COLLISION PROBABILITIES OF THE SSS FD SIGNALS BETWEEN INTERCELLS IN A SYNCHRONOUS ENVIRONMENT

	Single	Double	Triple	Quadruple
LTE	2.48%	0%	0%	0%
NR	0%	0%	0%	0%
AR	0%	0%	0%	0%

against CFO. The observation will be verified in Section VI. In addition, for reference, according to [15], the effect of the Doppler shift caused by mobility on system is almost equal to that of CFO on system, so that it can be said to be strong on Doppler shift as long as it is strong on CFO. But the relation between Doppler spread and CFO is unknown. This relation will be observed through a frequency-selective multipath channel model that reflects Doppler spread when making performance evaluation in Section VI.

G. Comparative Analysis Regarding SSS Specification

First, let us compare AR with LTE and NR as summarized in Table V in terms of collision probability whose effect on PCI acquisition accuracy is negative. Collision probability in case of LTE is calculated as the number of sequence sets C (i.e., total PCIs) is $Q \times G$, where each sequence set is composed of $S^e_{0,c}$, $S^o_{0,c}$, $S^e_{5,c}$, and $S^o_{5,c}$ for every frame. From (5), $S^e_{f',c}$ and $S^o_{f',c}$ stand for even and odd elements of $S_{f',c}$, respectively. In the table, "single," "double," "triple," and "quadruple" mean the number of hitting elements for a pair of $(S^e_{0,c}, S^o_{0,c}, S^e_{5,c}, S^o_{5,c})$ and $(S^e_{0,c'}, S^o_{0,c'}, S^e_{5,c'}, S^o_{5,c'})$ with $c \neq c'$ is 1, 2, 3, and 4, respectively. Also, collision probability in case of both NR and AR is calculated as in LTE except that each sequence set consists of only $S_{0,c}$ in each of (7) and (10) for every frame. Back to comparative analysis, in LTE, once again, the second scrambling sequences w_{i_0} and w_{i_1} in (5) are specified to average the intercell interference through escaping the double collision [19] as shown in the table. Besides, the intercell interference is further randomized by the first scrambling sequences e_0 and e_1 in (5) thanks to the number of randomization sets by a factor of 3, from 168 to 504. On the other hand, in NR and AR, there are not any collisions as shown in the table. No collision leads for the SSS signals of NR and AR to have the highest robustness to intercell interference, which will be observed in Section VI.

Second, let us compare AR with LTE and NR in terms of normalized cross correlation in the absence of multiple paths, fading, and AWGN as shown in Fig. 3. In this figure, "min," "mean," and "max" mean the lowest value, average value, and the highest value, respectively, among normalized cross-correlation outputs between one of all possible sequence sets from serving cell c and another from interfering cell $c'(\neq c)$. This analysis shows that while NR and AR provide almost the same correlation performance, both NR and AR outperform LTE in terms of all of min, mean, and max. Especially, it can be seen that there is a significant difference between NR/AR and LTE in terms

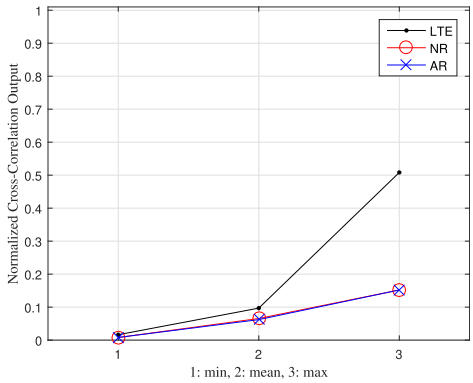

Fig. 3. Cross correlation performances of LTE, NR, and AR.

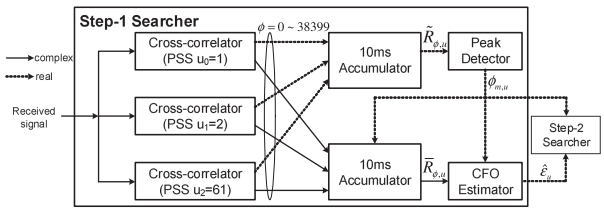

Fig. 4. Step-1 searcher.

of the highest correlation level, and this difference can have a significant impact on PCI acquisition performance, which will be observed in Section VI.

V. SEARCHER DESCRIPTION AND ANALYSIS

A. Step-1 Searcher

At an initial system-access setup, a receiver has to carry out noncoherent detection to acquire the starting sample time of PSS TD signal (SSTP) excluding CP (i.e., sample time offset (STO) is zero). According to [5] and [30], maximal cross correlation under automatic gain control [8] is regarded as maximum likelihood timing estimation [6]. For this ground, to maximize the correlation between the received signal and the preknown PSS signal to the receiver, Step-1 searcher for AR performs signal replica-correlation in time domain.

As shown in Fig. 4, Step-1 searcher constructs three cross correlators (each hypothesis of three PID indexes u), real-value 10-ms accumulator, complex-value 10-ms accumulator, peak detector, and CFO estimator. The complex-value(real-value) output $R_{\phi,u}(\breve{R}_{\phi,u})$ of cross correlator u for each sample time instant ϕ $(0 \leq \phi < 38400)$, where 38 400 is the number of samples coping with one frame duration, can be defined as

$$R_{\phi,u} = \sum_{a=0}^{A-1} \left\{ \frac{\left(\mathbf{x}^{c,6}_{0,f}\right)^* (\mathbf{r}^a_{l,f',f})^T(\phi)}{N} \right\}, \quad \breve{R}_{\phi,u} = |R_{\phi,u}| \quad (13)$$

where $\mathbf{x}^{c,6}_{0,f}$ is $1 \times N$ PSS TD vector shown in (2), and is specified as the time-domain version of (9). Also, $\mathbf{r}^a_{l,f',f}$ as shown in (3) is $1 \times N$ Rx signal vector which is related with the AR PSS. Moreover, the meaning of $\cdot(\phi)$ in $\mathbf{r}^a_{l,f',f}(\phi)$ is that the starting element of $\mathbf{r}^a_{l,f',f}$ in (3) is not from the starting sample time of effective OFDM symbol l at f' and f, but from the sample time instant ϕ. Also, the outputs $\bar{R}_{\phi,u_{\bar{c}}}$ and $\tilde{R}_{\phi,u_{\bar{c}}}$ of the complex-

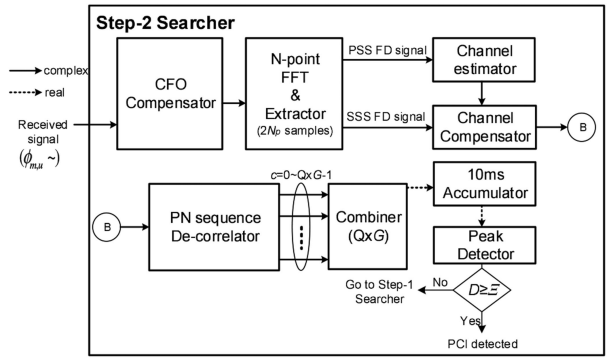

Fig. 5. Step-2 searcher.

and real-value 10-ms accumulators from (13) are defined as, respectively,

$$\bar{R}_{\phi,u} = \bar{R}_{\phi-T_p,u} + R_{\phi,u}, \quad \tilde{R}_{\phi,u} = \tilde{R}_{\phi-T_p,u} + \breve{R}_{\phi,u} \tag{14}$$

where T_p is the time-window size 10 ms of first-step searcher, and $\bar{R}_{\phi-T_p,u}$(or $\tilde{R}_{\phi-T_p,u}$) denotes the value saved in the previous time-window, and is replaced by $\bar{R}_{\phi,u}$(or $\tilde{R}_{\phi,u}$) in the current time-window. In sequel, $\bar{R}_{\phi,u}$ is named as decision variable (DV) for detecting SSTP. As shown in Fig. 4, $\tilde{R}_{\phi,u}$ is flowing into the input of the peak detector whose output $\phi_{m,u}$ is regarded as the SSTP estimated as the following criterion:

$$\phi_{m,u} = \arg\max_{\phi,u} \tilde{R}_{\phi,u} \tag{15}$$

where it is meant that STO $\theta = 0$ if $\phi_{m,u} =$ actual SSTP, which allows $\theta = 0$ to be replaced with $\phi = \phi_{m,u}$. After performing the peak detection, the proposed first-step searcher estimates CFO ε_u in the CFO estimator [17], [24] using $\phi_{m,u}$ and $\bar{R}_{\phi_m,u}$, where single CFO hypothesis (i.e., there is no integer CFO.) is assumed in this article.[11] Lastly, Step-1 searcher is done after $\phi_{m,u}$ and ε_c are reported to Step-2 searcher.

B. Step-2 Searcher

As shown in Fig. 5, Step-2 searcher consists of CFO compensator, N-point FFT & Extractor, channel estimator, channel compensator, PN sequence decorrelator, combiner, 10-ms accumulator, peak detector, and comparator.

First, CFO ε_u is compensated for the Rx signal $\sum_a \tilde{r}^a_{l,f',f}[n]$, in which equal gain combining Rx diversity is applied to the element of vector $\tilde{\mathbf{r}}^a_{l,f',f}$ in (3), from starting sample time $\phi_{m,u} - (N^6_{cp} + N)$ regarded as starting sample time of SSS FD signal excluding CP. Second, we perform N-point FFT for the compensated signals from starting $\phi_{m,u}$ regarded as starting sample time of PSS FD signal excluding CP. And then we make guard-band removing, that is, $(2N_p)$-sample extracting without dc subcarrier for each u. By doing these, we obtain the PSS FD signal $P_{\hat{f}',u}[k] (0 \le k < 2N_p)$ at subframe $\hat{f}'$ (assumed subframe 0 from Step-1 searcher) as shown in Fig. 1 with fading and noise. Third, the estimated channel state information $\hat{H}^u_{pss}[k]$ which is an estimated version of $\sum_a H^{c,a}_{6,\hat{f}',f}[k]$ in (3) is obtained based on discrete Fourier transform-based time-domain filtering algorithm [31]. Fourth, we get the extracted SSS FD signal $S_{\hat{f}',c}[k] (0 \le k < 2N_p)$ in the same manner as the estimated PSS FD signal. Fifth, $\hat{S}_{\hat{f}',c}[k] = (\hat{H}^u_{pss})^*[k] S_{\hat{f}',c}[k]$ in the output of channel compensator. Sixth, passing through PN sequence decorrelator [i.e., summated term in (16)], the combined signal for CGI g per PID u is obtained as

$$\tilde{S}(g,u) = \sum_{k=0}^{2N_p-1} \left\{ \hat{S}_{\hat{f}',c}[k] S_{0,c}[k] \right\}, \ 0 \le g < G, \ 0 \le u < Q \tag{16}$$

where $S_{0,c}$ is the preknown SSS FD signal to receiver, and stands for that in (10) with $c = 3g + u$. The output $\bar{S}(g,u)$ of 10 ms accumulator from (16) is defined as $\bar{S}(g,u) = \bar{S}(g, u - T_s) + \tilde{S}(g,u)$, where T_s is the time-window size 10 ms of second-step searcher, and $\bar{S}(g, u - T_p)$ replaced by $\bar{S}(g,u)$ in the current time-window denotes the value saved in the previous time-window. Seventh, as shown in Fig. 5, $\bar{S}(g,u)$ is flowing into the input of the peak detector whose output $(\hat{g}, \hat{u})$ is regarded as a set of CGI and PID detected as the following:

$$(\hat{g}, \hat{u}) = \arg\max_{g,u} \left\{ \bar{S}(g,u) \right\} \tag{17}$$

where it is meant that, from $(\hat{g}, \hat{u})$, $\phi_{m,\hat{u}}$ is the resultant STO estimated, and the final PCI $\hat{c}$ is $3\hat{g} + \hat{u}$. Lastly, decision metric D, another output of the peak detector, that is required for us to determine whether cell search is done or not is defined as

$$D = \frac{\left|\bar{S}(\hat{g},\hat{u})\right|}{\sum_{g \ne \hat{g}, u \ne \hat{u}} \left|\bar{S}(g,u)\right| / (G \times Q - 1)}. \tag{18}$$

If $D \ge \Xi$ with threshold level Ξ predefined, cell search is done. OW, go to the first-step searcher again. The denominator in (18) is likely to be the average power of the noise term such that D can be regarded as SNR. How come we use D instead of $|\bar{S}(\hat{g},\hat{u})|$ is that if we use D, then Ξ does not rely on automatic gain control level in the receiver [24].

TABLE VI
COMPARATIVELY COMPUTATIONAL COMPLEXITY FOR STEP-1 SEARCHER

	♯ operations	MOPS [μs]
LTE	$\approx 127N^3$	$0.0127N^3$
NR	$\approx 63N^3$	$0.0063N^3$
FD-version [18]	$\approx 63N^3$	$0.0063N^3$
AR	$\approx 33N^3$	$0.0033N^3$

C. Searcher Complexity

On one hand, the most computationally intensive part of cell search is in Step-1 searcher. As it is based on millions of operations per second (MOPS) [28], which is commonly used in the TFS complexity comparisons of LTE and NR standards. All of LTE, NR, FD-version [18], and AR is assumed to apply one common ML method as in (13)–(15) to their Step-1 searchers. According to this, comparatively computational complexities are outlined in Table VI,[12] where we assume 10 ms accumulation. From the table, the efficiency of AR is observed as the

[11] This assumption is intended to provide a fair comparison with LTE, where a maximum tolerable CFO of 5.05 ppm (i.e., less than 15 kHz) is used with a carrier frequency of less than 2 GHz and a subcarrier spacing of 15 kHz.

[12] In this article, the complexities of CFO estimator and peak detector as shown in Fig. 4 are excluded because they are employed to all of the schemes

TABLE VII
SSS GENERATION COMPLEXITY

	♯ seq generations	♯ BPSK modulations	♯ multiplications
LTE	6	6	6
NR	2	8	4
AR	2	4	0

MOPS of AR is 1.9 times lower than that of NR/FD-version [18] since the PSS TD signal of AR is real from Appendix A. Besides, AR has a computational reduction of 3.8 times over LTE if we let LTE have the same time-resolution as AR.

On the other hand, the complexity of Step-2 searcher is primarily related to the hardware that is required to generate SSS FD signal and to obtain the correlation output $\tilde{S}(g,u)$ in (16). First, let us compare AR with LTE and NR in terms of hardware complexity when generating SSS FD signals summarized in Table VII. In this table, we count one generation of PN sequence as one regardless of sequence length, one BPSK modulation of length-31 PN sequence sequence as one (e.g., ♯ BPSK modulations for one length-127 PN sequence is 4.), and one binary multiplication of two length-31 PN sequences as one (e.g., ♯ binary multiplications of two length-127 PN sequences is 4.). In detail, while both NR and AR need 2 sequence generations regarding x_0 and x_1, LTE needs 6 sequence generations regarding b_{i_0}, b_{i_1}, e_0, e_1, w_{i_0}, and w_{i_1}. Also, while AR needs only 4 BPSK modulations regarding $x_0 \oplus x_1$, NR needs 8 BPSK modulations regarding x_0 and x_1, and LTE needs 6 BPSK modulations regarding above 6 sequences. Moreover, while AR needs no binary multiplication, NR needs 4 binary multiplications regarding $[1-2x_0][1-2x_1]$, and LTE needs 6 binary multiplications regarding above 6 sequences. This hardware complexity analysis shows that AR may have the lowest hardware complexity by about three times compared to LTE and NR, although the difference is not large.

Second, let us compare AR with LTE and NR in terms of hardware complexity when getting correlation output for acquiring PCI. AR only requires one decorrelator from Fig. 5 and (16), while LTE needs ten descramblers and nine decorrelator banks to perform Step-two searching [24], and NR needs two decorrelators from (7). If we consider that the receiver is required to often perform neighbor cell search in order to guarantee successful handover, the running time of Step-1 and Step-2 searchers may be longer than any other modules in the baseband modem. Thus, the results of these hardware complexity analyses show that AR has the lowest hardware complexity, that is, at least ten-times and two-times complexity reduction over LTE and NR, respectively, when roughly qualitatively aggregated. Consequently, we are able to minimize battery consumption by reducing the hardware complexity in the second-step searcher as well as computational complexity in Step-1 searcher.

D. Average Cell-Search Time Analysis

On the basis of a Markovian model suitable for a single-dwell search procedure [32], we analyze average search time (AST). To realize reasonable match with this model, mobile velocities of more than 250 km/h can be assumed since these velocities allow the SS block for each frame to experience mutually independent fading. In the single-dwell procedure, we fix the time durations T_p and T_s for Step-1 and Step-2 searchers to be constant, respectively, so that single dwell time is $T = T_p + T_s$. In this analysis, we set $T_p = 10$ ms $\times\, \Upsilon$ and $T_s = 10$ ms $\times\, \Upsilon$ according to accumulation length [10 ms] Υ. The state diagram plotted in Fig. 6 illustrates cell search process and corresponding state diagram on single dwell. The levels on branches between states (nodes) indicate the probability of each transition, multiplied by a power of the abstract variable Z used to determine the transfer function of the state diagram. The power is utilized to indicate the hypothesis testing time periods needed to make the given transition [33]. In Fig. 6, P_D, P_M, and P_F are the detection, misdetection, and false alarm probabilities, respectively, as the following definition: $P_D =$ Pr{Both Step searchers are correct, and $D \geq \Xi$ in (18)}; $P_M =$Pr{$D < \Xi$ in (18)}; and $P_F =$Pr{One(or both) of Step-1 and Step-2 searchers is incorrect, but $D \geq \Xi$ in (18)}.

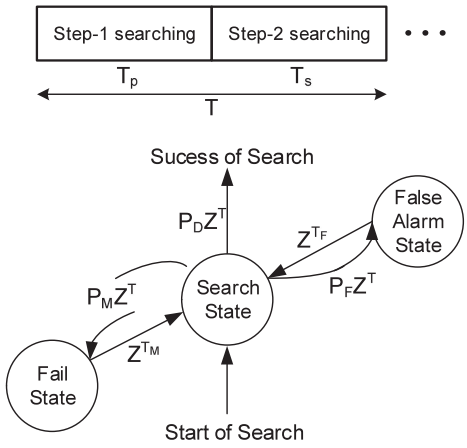

Fig. 6. Single dwell cell search process and corresponding state diagram.

It is noteworthy that $P_D + P_M + P_F = 1$, T_F is the false alarm time, and T_M is the time to perform a failure detection. Note also that T_F is set to be 100 ms as in [17], [24]. However we set a nonzero T_M to be 5 ms unlike in [24]. Since T_F always takes much longer for the searcher to realize that it establishes a wrong connection than to realize that it cannot establish a connection. From the two-step cell-search strategy mentioned in Sections V-A and V-B as well as the state diagram, we can deduce that its transfer function is

$$U(Z) = \frac{P_D Z^T}{1 - P_M Z^T Z^{T_M} - P_F Z^T Z^{T_F}}. \tag{19}$$

Finally, the average cell search time is

$$E\{T_{avg}\} = \frac{dU(Z)}{dZ}\Big|_{Z=1} = \frac{T + T_M P_M + T_F P_F}{P_D} \tag{20}$$

where $P_D = P_{D1} P_{D2|H1}$ and $P_F = P_{D1} P_{M2|H1} + (1 - P_{D1}) P_{M2|H0}$.$P_{D1}$, $P_{D2|H1}$, $P_{M2|H1}$, and $P_{M2|H0}$ are defined as

$P_{D1} =$ Pr{PID $\hat{u}$ detected in Step-1 searcher is identical to the transmitted one, and the difference between the detected STO and the real STO is within $\pm\lfloor N_{cp}^6/2 \rfloor$};

considered. In addition, since operation count depends on operation set architecture in practical MOPS metric, the computational number of one real addition, one real multiplication, and one squared root is assumed to 1, 8, and 6 operations, respectively, from which the complexities of complex addition and multiplication are calculated.

$P_{D2|H1} = \Pr\{$PCI $\hat{c}$ detected in Step-2 searcher is correct, and $D \geq \Xi$ in (18) in the case when the detection in Step-1 searcher is correct$\}$;

$P_{M2|H1} = \Pr\{$PCI $\hat{c}$ detected in Step-2 searcher is incorrect, but $D \geq \Xi$ in (18) in the case when the detection in Step-1 searcher is correct$\}$, and

$P_{M2|H0} = \Pr\{D \geq \Xi$ in (18) in the case when the detection in Step-1 searcher is incorrect$\}$.

VI. Performance Evaluation

This section observes multifarious performances in the presence of 5.05 ppm CFO [22] and 500 km/h mobility [23]. The observed performances are evaluated with physical-layer LTE and NR specifications [1], [4] and the following parameter settings: A common carrier frequency of 2 GHz; no Tx diversity is assumed, but two branch Rx equal gain combining diversity [i.e., $A = 2$ in (3)] is adopted; the TU-6 channel [29] is adopted as a channel model with mobile velocities of 3, 250, and 500 km/h;[13] a two-cell model comprising a serving cell and a dominant interfering cell is employed where two cells are configured with different PCIs and PIDs; the signal arrival time difference of adjacent cell relative to serving cell is assumed to be uniformly distributed within [3, 3] μs; subcarrier spacing is 15 kHz as in LTE; and while both 10ms-length accumulation and 20 ms-length accumulation are employed. According to synchronization signal description mentioned in Section IV, in case of 10 ms-length accumulation, while one-time accumulation is made in LTE, no accumulation is made in NR, [18], and AR. In case of 20 ms-length accumulation, 3-time and 1-time accumulations are realized in LTE and all of NR, [18], and AR, respectively. Also, letting I_D denote the average power of the dominant interfering cell, it is assumed for E_s to be identical to I_D to observe performance in the worst case environment, and SNR is set to be E_s/N_0. Moreover, all of the feasible subcarriers corresponding to other channels are always loaded (i.e., full system load), and the transmission power for each of the PSS and SSS signals is identical to that for each of other channels.

A. Per-Step DER

Fig. 7 shows the DER performances regarding Step-1 searching algorithms employing 10ms-length accumulation and 20ms-length accumulation, respectively, as a function of SNR per Rx antenna. To observe a worst case in this figure, we set CFO ε_c to be 0.6733 corresponding to 5.05 ppm(=10.1 kHz) [22], and mobile velocities to be 3, 250, and 500 km/h [23]. When we evaluate DER, if the detected timing is not only within half of absolute CP duration but also the detected PSS sequence index $\hat{u}$ is correct, a successful detection is declared. OW, an error is declared. From the results of this figure, it is observed as follows. 1) As accumulation length increases, DER improvement is observed for all because of more time diversity gain although affected by ICI as the mobile velocity increases. (2) While LTE is not functional and NR may be operational but not enough, AR is shown to be capable of making valuable robustness against CFO and mobility. 3) FD-version [18] is between LTE and NR in terms of DER performance, which is in the same line as Table IV in Section IV-F. 4) DER degradation

[13] Since LTE is included in the comparison, corresponding maximum Doppler frequency to given mobility is varied based on 2 GHz carrier frequency in the TU-6 channel model.

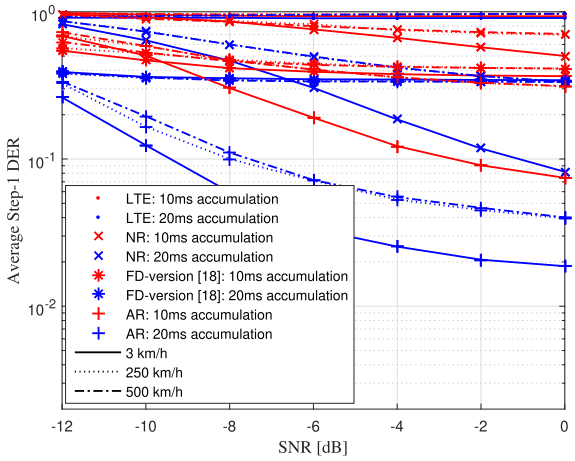

Fig. 7. Step-1 DER vs. SNR with a high CFO of 5.05 ppm.

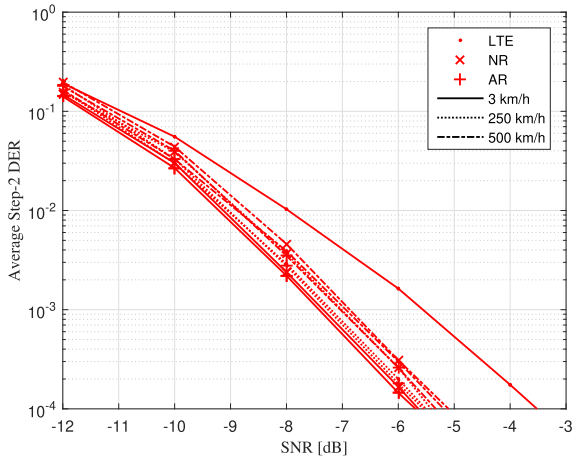

Fig. 8. Step-2 DER vs. SNR with 10-ms accumulation length for a low CFO of 0.15 ppm.

is observed more and more for all schemes as mobile velocity increases because the negative effect of the ICI resulting from mobile velocity on DER performance increases as well. 5) In case of 10ms-length accumulation in Fig. 7, LTE may expect more DER improvement because of more time diversity gain according to increasing mobile velocity. That is specifically coming from the fact that NR, FD-version [18], and AR are not able to anticipate any time diversity gain [17], [24], while LTE is capable of doing this. According to the assumption that no accumulation are employed in NR, FD-version [18], while LTE is capable of employing one-time accumulation. However, it is observed that the opposite is true since LTE has a very vulnerable characteristic to CFOs.

Figs. 8 and 9 show the DER performances regarding Step-2 searching algorithms as a function of SNR per Rx antenna with 10-ms accumulation and 20-ms accumulation lengths, respectively. In these figures, in order to be observed in a worst case with up-to 500 km/h mobility, we set the residual CFO ε_c to 0.02 corresponding to 0.15 ppm(=300 Hz), as well as a residual STO that is uniformly distributed in $[-\lfloor N_{cp}^6/2 \rfloor, +\lfloor N_{cp}^6/2 \rfloor]$. When evaluating these DERs, we assume that the PSS sequence detection is correct in Step-1 searcher, and Step-2

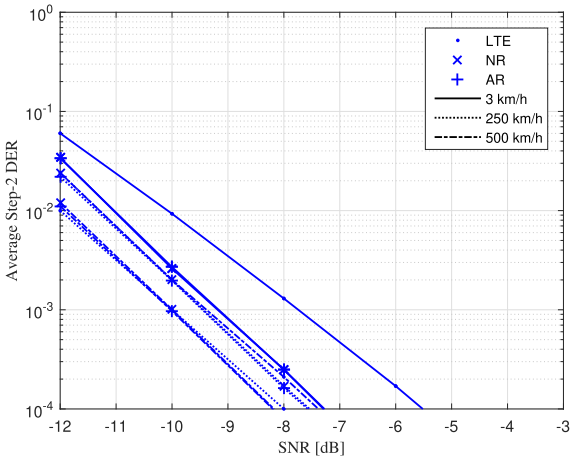

Fig. 9. Step-2 DER vs. SNR with 20-ms accumulation length for a low CFO of 0.15 ppm.

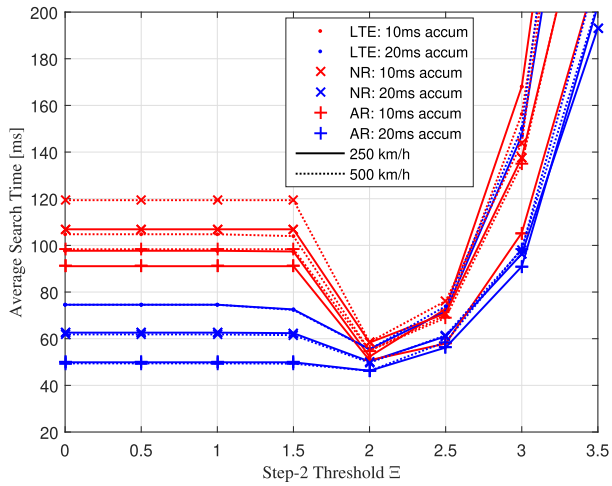

Fig. 10. AST vs. Step-2 threshold at SNR $= -10$ dB.

threshold Ξ defined in (18) is zero,[14] but practical channel estimation/recovering is employed. Also, if all of the PCI (in case of all of LTE, NR, and AR) and frame synchronization (in case of LTE alone) are correct, a successful detection is declared. OW, an error is declared. From the results of these figures, it is observed as follows. 1) Over the entire performance case, both NR and AR provide very similar performances to each other. 2) For 10-ms accumulation length at 3 km/h in Fig. 8, both NR and AR outperform LTE in terms of DER performance. In this case, even though LTE is capable of making one-time accumulation unlike NR and AR once again, it is analyzed that 5 ms accumulation interval in LTE is too short to achieve any time diversity gain. 3) For 10-ms accumulation length in Fig. 8, as mobile velocity increases, DER improvement is observed owing to dominant time diversity gain in LTE although affected by ICI as the mobile velocity increases. On the contrary, as mobile velocity increases, DER degradation is observed more and more for NR and AR because of the impact of ICI with no time diversity by no accumulation. 4) For 20-ms accumulation length at 3 km/h in Fig. 9, both NR and AR provide the SNR gain of more than 1 dB compared to LTE since it is analyzed that this accumulation interval in NR and AR is enough to benefit from time diversity gain. 5) For 20-ms accumulation length in Fig. 9 as mobile velocity increases from 250 to 500 km/h, it can be observed that the DER performance of LTE is rather impaired due to its impact on ICI. On the contrary, it can be observed that the DER performances of NR and AR are rather improved due to the overwhelming time diversity gain despite the negative impact on ICI.

B. Average Search Time

Fig. 10 shows AST performance according to Step-2 threshold under an initial CFO that is uniformly distributed in [−5.05 ppm, +5.05 ppm] under the assumption that P_{D1}, $P_{D2|H1}$, $P_{M1|H1}$, and $P_{M2|H0}$ are obtained through simulation. It is observed that the proposed scheme outperforms existing schemes. From the observations of Fig. 7, for a very higher fractional CFO, the proposed scheme shows remarkable robustness over LTE and NR. In addition, each AST level of LTE, NR, and AR is almost constant for thresholds as large as 1.5, with a threshold of 2.0 showing a common weak minimum. Moreover, the proposed scheme can be said not only to support mobility up to 500 km/h but also to overcome ICI as a result of increased mobility by applying PSS accumulation. Furthermore, in case of a fixed CFO of 5.05 ppm as a worst case scenario, it is obvious that the performance gaps between the proposed scheme and existing ones will widen further from Fig. 7 as well.

[14]It is noted that the effect of this threshold on cell-search time will be evaluated in Section VI-B.

VII. Conclusion

This article proposed a couple of synchronization signals for cell search. For time/frequnency synchronization and partial cell identification, the first proposed signal reduced computational complexity by a factor of 1/2 and provided a much robust CFO/mobility against existing PSS signals of LTE and NR. For final PCI detection, the second proposed signal minimized intercell interference. Our comparative evaluation elucidates that as in NR, the second proposed signal shares commonly multiple advantages of zeroing collision probability and minimizing high cross correlation among PCI signals which results in very higher accuracy of PCI detection over LTE. However, as mobile velocity increases, it should not be overlooked that time diversity gain by means of accumulation is an important factor in improving cell-search accuracy. In general, it is true that the short average cell-search time in conjunction with lower searcher complexity results in slower battery consumption and higher power efficiency. From this fact, the improved performance presented in this investigation will provide useful information on designing synchronization signals in OFDM-based wireless systems.

Appendix

A. Proof of Proposition 1

Substituting (9) into $\tilde{x}_{0,f}^{c,6}[n]$ in (1), we have the PSS TD signal as

$$\tilde{x}_{0,f}^{c,6}[n] = \sum_{k=1}^{N_p} \left\{ P_{0,u}[k+N_p] e^{j\frac{2\pi nk}{N}} + P_{0,u}[N_p-k] e^{-j\frac{2\pi nk}{N}} \right\}$$

$$= \sum_{k=1}^{N_p} \left\{ \begin{array}{l} \underbrace{(P_{0,u}[k+N_p]+P_{0,u}[N_p-k])}_{A[k]} \cos\left(\frac{2\pi nk}{N}\right) \\ +j \underbrace{(P_{0,u}[k+N_p]-P_{0,u}[N_p-k])}_{B[k]} \sin\left(\frac{2\pi nk}{N}\right) \end{array} \right\}. \tag{21}$$

Based on a fact that $P_{0,u}[k+N_p] = P^*_{0,u}[N_p-k]$ from (9), the first term of the second line in (21) is real because $A[k] = 2\text{Real}\{P_{0,u}[k-N_p]\}$. Also, the second term is real because $B[k] = j2\text{Imag}\{P_{0,u}[k-N_p]\}$. Thus, the value of $\tilde{x}^{c,6}_{0,f}[n]$ is real for all n's.

REFERENCES

[1] 3GPP TSG RAN, "Physical channels and modulation (Release 13)," France, 3GPP, TS36.211 v13.5.0, pp. 125–128, Mar. 2017.

[2] 3GPP TSG RAN, "Channel coding (Release 13)," France, 3GPP, TS36.212 v13.1.0, Mar. 2016.

[3] 3GPP TSG RAN, "Physical layer procedures (Release 13)," France, 3GPP, TS38.211 v15.2.0 Jun. 2017.

[4] 3GPP TSG RAN, "Physical channels and modulation (Release 15)," France, 3GPP, TS38.211 v15.2.0, Jun. 2018.

[5] J. J. van de Beek, M. Sandell, P.O. Börjesson, "ML estimation of time and frequency offset in OFDM systems," *IEEE Trans. Signal Process.*, vol. 45, no. 7, pp. 1800–1805, Jul. 1997.

[6] I. Toufik, S. Sesia, and M. Baker, *LTE - The UMTS Long Term Evolution: From Theory to Practice*, New York, NY, USA: Wiley, 2009.

[7] M. M. Mansour, "Optimized architecture for computing Zadoff-Chu sequences with application to LTE," in *Proc. IEEE Globecom Telecommun. Conf.*, 2009.

[8] W. Xu and K. Manolakis, "Robust synchronization for 3GPP LTE systems," in *IEEE Globecom Telecommun. Conf.*, 2010.

[9] Z. Zhang, K. Long, and Y. Liu, "Complex efficient carrier frequency offset estimation algorithm in OFDM systems," *IEEE Trans. Broadcast*, vol. 50, no. 2, pp. 159–164, Jun. 2004.

[10] J. Yuan and M. Torlak, "Joint CFO and SFO estimator for OFDM receiver using common reference frequency," *IEEE Trans. Broadcast.*, vol. 62, no. 1, pp. 141–149, Mar. 2016.

[11] M. Morelli and M. Moretti, "A robust maximum likelihood scheme for PSS detection and integer frequency offset recovery in LTE systems," *IEEE Trans. Wireless Commun.*, vol. 15, no. 2, pp. 1353–1363, Feb. 2016.

[12] J.-C. Lin, Y.-T. Sun, and H. V. Poor, "Initial synchronization exploiting inherent diversity for the LTE sector search process," *IEEE Trans. Wireless Commun.*, vol. 15, no. 2, pp. 1114–1128, Feb. 2016.

[13] C. Hu and Y. Zhang, "5 G NR Primary Synchronization Signal Detection with Low Hardware Resource Occupancy," in *Proc. IEEE Int. Conf. Commun. China*, 2018, pp. 304–308.

[14] H. Abdzadeh-Ziabari, W.-P. Zhu, and M. N. S. Swamy, "Joint maximum likelihood timing, frequency offset, and doubly selective channel estimation for OFDM systems," *IEEE Trans. Veh. Technol.*, vol. 67, no. 3, pp. 2787–2791, Mar. 2018.

[15] R. Zeng, H. Huang, L. Yang, and Z. Zhang, "Joint estimation of frequency offset and Doppler shift in high mobility environments based on orthogonal angle domain subspace projection," *IEEE Trans. Veh. Technol.*, vol. 67, no. 3, pp. 2254–2266, Mar. 2018.

[16] K. Chang and Y. Han, "Robust replica correlation-based symbol synchronization in OFDM systems," *Electron. Lett.*, vol. 44, no. 17, pp. 1024–1025, Aug. 2008.

[17] K. Chang, P. Ho, and Y. Choi, "Signal design for reduced-complexity and accurate cell-search/synchronization in OFDM-based cellular systems," *IEEE Trans. Veh. Technol.*, vol. 61, no. 9, pp. 4170–4174, Nov. 2012.

[18] M. M. U. Gul, X. Ma, and S. Lee, "Timing and frequency synchronization for OFDM downlink transmissions using Zadoff-Chu sequences," *IEEE Trans. Wireless Commun.*, vol. 14, no. 3, pp. 1716–1729, Mar. 2015.

[19] 3GPP TSG RAN WG1, "Scrambling Method for Two S-SCH Short Code," Motorola, Tdoc R1-072661, Meeting #49bis, Jun. 2007.

[20] J. Myung, J. Kang, Y. Baek, and B. Koo, "Efficient S-SCH detection algorithm for LTE downlink channel," in *Proc. IEEE Trans. Veh. Technol.*, vol. 63, no. 6, pp. 2969–2973, Jul. 2014.

[21] M. Morelli and M. Moretti, "A maximum likelihood approach for SSS detection in LTE systems," *IEEE Trans. Wireless Commun.*, vol. 16, no. 4, pp. 2423–2433, Apr. 2017.

[22] P. Wang and F. Berggren, "Secondary synchronization signal in 5 G New Radio," in *Proc. IEEE Int. Conf. Commun.*, May 2018.

[23] A. Omri, M. Shaqfeh, A. Ali, and H. Alnuweiri, "Synchronization procedure in 5 G NR systems," *IEEE Access*, vol. 7, pp. 41286–41295, Mar. 2019.

[24] I. Kim, Y. Han, and H. K. Chung, "An efficient synchronization signal structure for OFDM-based cellular systems," *IEEE Trans. Wireless Commun.*, vol. 9, no. 1, pp. 99–105, Jan. 2010.

[25] K. Chang, K. Kim, and D. H. Kim, "Reduction of Doppler effects in OFDM systems," *IEEE Trans. Consum. Electron.*, vol. 52, no. 4, pp. 1159–1166, Nov. 2006.

[26] Savo Glisic, *Advanced Wireless Communications: 4G Technologies*, Hoboken, NJ, USA: Wiley, 2004.

[27] M. Speth, F. Classen, and H. Meyr, "Frame synchronization of OFDM systems in frequency selective fading channels," in *Proc. IEEE 47th Veh. Technol. Conf. Technol. Motion*, vol. 3, 1997, pp. 1807–1811.

[28] 3GPP TSG RAN WG1, "On device complexity for NB-IoT cell search," Intel, Tdoc R1-155853, Meeting #82bis, October 2015.

[29] 3GPP, "Technical specification group radio access networks; Deployment aspects," France, 3GPP, TR25.943 v8.0.0, Dec. 2008.

[30] H. Meyr, M. Moeneclaey, and S.A. Fechtel, *Digital Communication Receivers: Synchronization, Channel Estimation, and Signal Processing*, Hoboken, NJ, USA: Wiley, 2001.

[31] 3GPP TSG RAN WG1, "Comparision of sequence and structure for P-SCH," LG Electronics, Tdoc R1-071531, Meeting #48bis, Mar. 2007.

[32] A. Polydoros and C. L. Weber, "A unified approach to serial search spread spectrum acquisition-Part I: General theory," *IEEE Trans. Commun.*, vol. COM-32, no. 5, pp. 542–549, May 1984.

[33] A. J. Viterbi, *CDMA: Principles of Spread Spectrum Communications*, Reading, MA, USA: Addison-Wesley, ch. 3, 1995.

Kapseok Chang received the M.S. and Ph.D. degrees in information and communications engineering from the Korea Advanced Institute of Science and Technology (KAIST), Daejeon, South Korea, in 1999 and 2005, respectively.

Since July 2005, he has been with Electronics and Telecommunications Research Institute (ETRI), Daejeon, South Korea as a Full-Time Senior Researcher. Since September 2009, he has also been an Associate Professor of Mobile Communication and Digital Broadcasting Engineering with University of Science and Technology (UST), South Korea. From March 2011 to February 2013, he was with the School of Engineering Science, Simon Fraser University, Burnaby, Canada as a Visiting Professor. His research interests include smart antennas, OFDM, synchronization, interference cancellation, in-band full-duplex (IFD) realization, and cellular IoT system. He made the standardization activities of 3GPP LTE (2005–2007) and IEEE 802.11ad (2009–2010), he developed the prototype of IFD system (2014–2015).

Dr. Chang was the recipeint of the Brain Korea Scholarship, during his Ph.D. He was the recipient of the Certificate of Appreciation, the Day of the Inventions, and the Best Patent Award, from IEEE 802.11ad (2012), Korean Ministry of Commerce, Industry and Energy (2018), and Electronics and Telecommunications Research Institute (2019), respectively.

Sangho Lee (Member, IEEE) received the B.S. degree in electronics engineering from Kyungpook National University, Daegu, South Korea, in 1988. He received the M.S. and Ph.D. degrees in information and communications engineering from Hannam University, Daejeon, South Korea, in 1998 and 2002, respectively.

From 1988 to 1993, he was a Research Engineer with Samsung Electronics and worked on switching system development. Since 1994, he has been with Electronics and Telecommunications Research Institute (ETRI), Daejeon, South Korea, as a Full-Time Senior Researcher. Between 2011 and 2012, he was with Chungcheong Leading Industry Office, South Korea, as a Project Director and in charge of wireless communications leading project. From 2015 to 2016, he was with the Department of Electrical and Computer Engineering, University of California, San Diego (UCSD) as a Visiting Scholar. He is currently managing the project planning for 6 G. His research interests include future mobile network architecture design and high-precision wireless communication technology.